Minerals Engineering 202 (2023) 108236

Contents lists available at ScienceDirect

Minerals Engineering

journal homepage: www.elsevier.com/locate/mineng

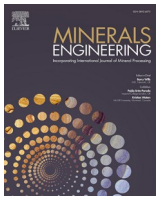

The effects of saline water on the recovery of lead and zinc sulfide during froth flotation

Anna M. Nowosielska [a], Aleksandar N. Nikoloski [a], Drew F. Parsons [a,b,*]

[a] Harry Butler Institute (Centre for Water, Energy and Waste), College of Science, Health, Engineering and Education (Engineering and Energy), Murdoch University, 90 South St, Murdoch, WA 6150, Australia
[b] Department of Chemical and Geological Sciences, University of Cagliari, Cittadella Universitaria, 09042 Monserrato, CA, Italy

ARTICLE INFO

Keywords:
Flotation
Sulfide minerals
Bubble
Zeta potential
Chemisoprtion

ABSTRACT

In this study, we investigated the effects of water salinity on the flotation performance of pure lead and zinc sulfide mineral samples as well as a Pb/Zn complex sulfide ore by means of micro-flotation and batch flotation experiments. Our results showed higher PbS and ZnS recoveries in more concentrated NaCl salt solutions. The results for the experiments using seawater demonstrated that in the presence of additional ions, such as Ca^{2+} and Mg^{2+}, the recovery of PbS and ZnS was significantly reduced.

As part of this investigation, we developed and implemented a surface complexation model for ZnS based on the presence of two differently charged surface sites. Zeta potential measurements of ZnS particles were used to optimise the parameters of our model. It was found that the surface potentials calculated using this model were in good agreement with the experimental zeta potentials, validating the model for predicting the zeta potential behaviour of ZnS particles over a broad range of pH and NaCl concentrations.

Additionally, total interaction free energies were determined as a function of separation distance, representing particle–particle and particle-bubble interactions of our study in different NaCl concentrations. The theoretical analyses showed that asymmetric Pb/Zn particle–particle interactions were repulsive at lower NaCl concentrations, before becoming purely attractive at higher NaCl concentrations. For the case of the symmetric particle–particle interactions, attraction controlled all interactions, regardless of NaCl concentration. The calculated PbS-bubble interactions were repulsive in lower NaCl concentrations but became increasingly attractive in higher NaCl concentrations. Strong repulsions controlled all ZnS-bubble interactions, and these interactions remained repulsive with increasing NaCl concentration. The theoretical projections presented in this study were in good agreement with the measured saline water flotation phenomena.

1. Introduction

Flotation is a widely applied technique for separating and concentrating ores based on their wettability properties. It is a complex three-stage process, which involves particle-bubble collisions, particle-bubble attachments, and the formation of stable particle-bubble aggregates (Dai et al., 2000). Since all particle-bubble interactions during flotation take place inside an aqueous medium, water chemistry plays a crucial role in controlling the nature of these interactions.

Due to the limited availability of freshwater in some parts of the world, seawater and/or recycled water with a higher salinity have become increasingly important for use in flotation. Several studies have documented the positive effects of inorganic electrolytes on flotation efficiency, which were attributed to the destabilizing effects of electrolytes on the hydration layers around the particles (Klassen and Mokrousov, 1963), and a reduced bubble coalescence (Craig et al., 1993a; 1993b) leading to an improved flotation rate (Marrucci and Nicodemo, 1967; Nowosielska et al., 2022). Increased flotation efficiency has also been linked with shorter induction times observed in more concentrated electrolyte solutions (Blake and Kitchener, 1973), as well as with a reduction of particle and bubble zeta potentials, resulting from a compression of the ionic diffuse layers in higher salt concentrations (Hancer et al., 2001; Castro et al., 2013; Nowosielska et al., 2022).

Lead sulfide (PbS) is the world's primary source for lead, which is used in energy storage systems associated with power generation. The mineral contains an equal amount of Pb^{2+} and S^{2-} ions, in a cubic

* Corresponding author.
E-mail address: drew.parsons@unica.it (D.F. Parsons).

https://doi.org/10.1016/j.mineng.2023.108236
Received 10 November 2022; Received in revised form 3 July 2023; Accepted 4 July 2023
Available online 22 July 2023

structure. Zinc sulfide (ZnS) is a main source of zinc metal. It occurs as two polymorphs: a cubic sphalerite or a hexagonal wurtzite. The mineral is mainly used in protective coatings for iron and steel.

Flotation separation and mineral recovery of lead and zinc from an ore where these two minerals co-exist is a complex process. In most operations, lead (Pb) concentrate will need to be treated and recovered from the ore before the zinc (Zn) concentrate can be successfully recovered via flotation (Huang et al., 2019). This multi-stage process is made possible due to the hydrophobic nature of PbS and the fact that ZnS is generally poorly collected by flotation reagents (Morey et al., 2001; Trahar et al., 1997).

Given that most sulfide ores contain lead (Pb) and zinc (Zn) mixed in together, to gain a better understanding of the fundamental particle-bubble interactions and to maximise their individual metal recoveries, it is important to initially study each mineral separately. Therefore, the aim of this current work was to investigate the effects of NaCl on the flotation of PbS and ZnS independently, and when they are contained within the same ore body.

The micro-flotation experiments were carried out on pure PbS and ZnS mineral samples, using solutions containing 1, 10 and 100 mM NaCl, at pH 9 (±0.1). The batch flotation experiments on a complex Pb/Zn sulfide ore were performed using solutions with NaCl concentrations of 1, 10, 100 and 500 mM, as well as seawater, at pH 9 (±0.1). A total interaction free energy for the interactions at different NaCl concentrations was calculated. The experimental results were then compared with the theoretical predictions representing particle-bubble and particle–particle interactions at two different NaCl concentrations, namely 10 and 500 mM, with the latter simulating the average NaCl concentration in seawater. The outcome of this work not only adds to the fundamental understanding of the effects of inorganic salts on the flotation of lead and zinc sulfide, but also provides more insight into a Pb/Zn complex sulfide ore flotation using saline water.

2. Experimental and theoretical

2.1. Materials

Pure PbS and ZnS mineral samples were used in micro-flotation experiments. X-ray diffraction (XRD) and a multi-elemental analysis by Inductively Coupled Plasma – Mass Spectrometry (ICP-MS) were used to verify the purity of these mineral samples. The XRD pattern in Fig. 1, (left), indicated a high purity PbS sample, with a chemical composition (wt %) of 85.61% Pb and 13.52% S. The XRD analysis in Fig. 1 (right), confirmed that the ZnS sample was wurtzite ((Zn,Fe)S), a less frequently encountered hexagonal polymorph of sphalerite, with a chemical composition (wt %) of 58.7% Zn, 6.2% Fe and 35.1% S. The Pb/Zn complex sulfide ore had a chemical composition of (wt %) 8.38% Pb and 8.68% Zn.

Deionised (DI) water was used in all experiments. Analytical grade sodium chloride (NaCl) was used to adjust the ionic strength of solution and sodium hydroxide (NaOH) and hydrochloric acid (HCl) of analytical grade used to regulate solution pH. The aqua regia solution, which was used for the digestion of the solid fractions before ICP-MS analyses, consisted of a mixture of nitric acid (HNO_3) and hydrochloric acid (HCl), both of analytical grade, in a molar ratio of 1:3. The major ion composition of the seawater used in the batch flotation experiments is detailed in Table 1. The concentration of NaCl in the seawater was ~ 510 mM.

The particle size distributions for lead sulfide, zinc sulfide and the Pb/Zn complex sulfide ore were determined by laser diffraction (Microtrac S3500) and are illustrated in Fig. 2. Table 2 shows the percentile points calculated using the Micro FLEX Software (Microtrac, Inc), in microns, which show the percentage of the volume that is smaller than the indicated size (see Table 3).

2.2. Micro-flotation experiments

The micro-flotation experiments were performed using a Hallimond tube with air as a bubble source. When not being tested, lead and zinc sulfide samples were stored in a freezer. Shortly prior to the experiments a small amount of the dry feed material was ground using a ceramic mortar and pestle. Each micro-flotation experiment was carried out on around 3 g of pure mineral particles (lead or zinc sulfide), suspended in 250 mL of the test solution. The test solution was prepared using DI water which also contained either 1, 10 or 100 mM NaCl. The pH in each test was adjusted to 9 (±0.1), with NaOH. The pulp was transferred to a Hallimond tube where it was conditioned for 3 min. The pulp was then aerated for 10 min with air at a flow rate of 70 cc/min (~4.2 L/Hr). The froth concentrates and the tailings were recovered, filtered, and dried. For each experiment, the mineral recovery was calculated from the solid

Table 1
Major ion composition of the seawater used in this study.

Ion	Concentration (mg/L)
Chloride (Cl^-)	19,000
Sodium (Na^+)	11,000
Calcium (Ca^{2+})	450
Magnesium (Mg^{2+})	1300
Potassium (K^+)	440
Sulfate (SO_4^{2-})	2570

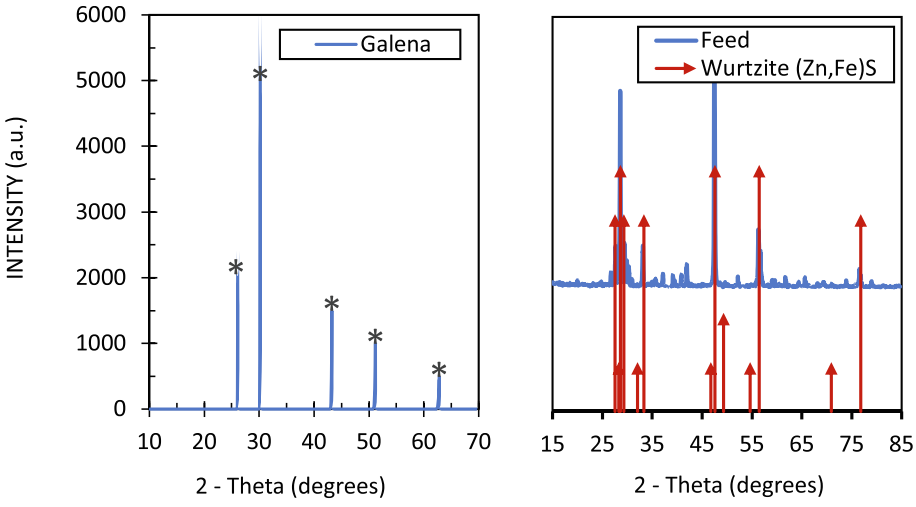

Fig. 1. X-ray diffraction pattern of PbS (left) and ZnS (right) samples used in this study.

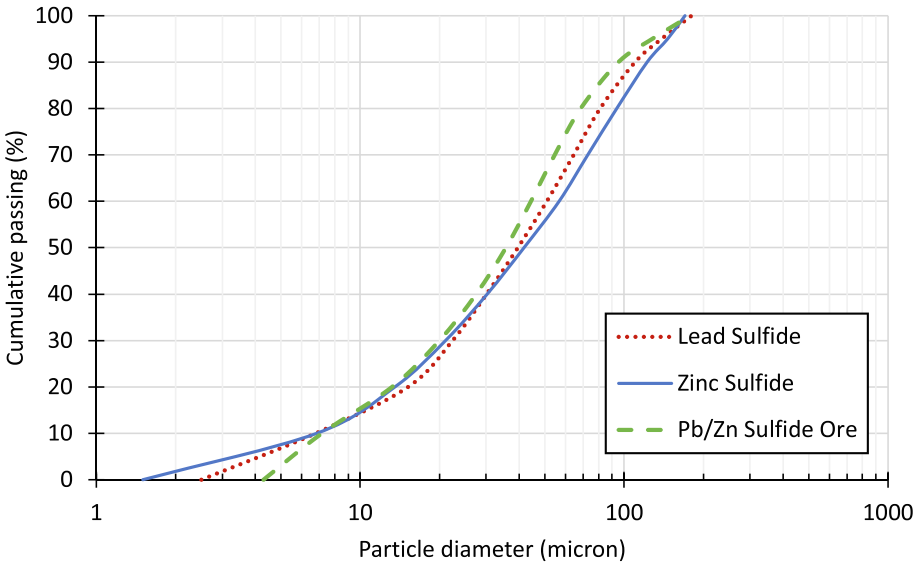

Fig. 2. Particle size distribution of the lead sulfide, zinc sulfide and the Pb/Zn sulfide ore samples used in the study.

Table 2
Calculated percentiles (percentage of volume) of the lead sulfide, zinc sulfide and Pb/Zn sulfide ore particles which are smaller than the indicated size.

Percentile (%)	Particle Diameter (μm)		
	Lead Sulfide	Zinc Sulfide	Pb/Zn Sulfide Ore
10	6.78	6.84	7.16
50	39.56	41.72	35.64
80	81.08	93.71	68.41
95	138.50	146.10	127.70
MV	43.17	54.99	46.04

Table 3
Parameters used to fit the chemisorption model for PbS calibrated using the measured zeta potentials (PbS zeta potentials in 10 mM NaCl).

PARAMETER	VALUE
N_S negative (sites m^{-2})	1.519×10^{16}
N_S neutral (sites m^{-2})	2.765×10^{16}
pK_{H1}	5.265
pK_{H2}	2.393
pK_{Na}	−2.376
pK_{Cl}	7.911

Table 4
Parameters used to fit the chemisorption model for ZnS, calibrated using the measured zeta potentials (ZnS zeta potentials in 10 mM NaCl).

PARAMETER	VALUE
N_S negative(sites m^{-2})	3.523×10^{16}
N_S neutral(sites m^{-2})	4.791×10^{16}
pK_{H1}	4.977
pK_{H2}	6.227
pK_{Na}	4.835
pK_{Cl}	3.016

mass of the froth concentrate and tailings and is presented as a recovery percentage (%). During filtration each fraction (concentrates and tailings) was additionally rinsed with DI water to minimise any salt precipitation once samples were dry. Fig. 3 illustrates the Hallimond tube setup used in the micro-flotation experiments.

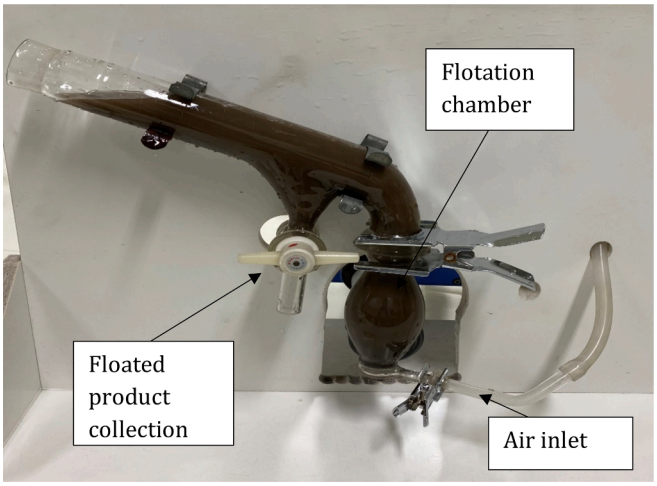

Fig. 3. Micro-flotation experimental set-up using a Hallimond tube.

Using the results from the micro-flotation experiments we applied the Klimpel model Eq. (1) (Fuerstenau et al., 2007) to calculate the first-order rate constants k(s^{-1}) as well as the maximum recovery R_m (%) for each test condition, according to the following:

$$R_t = R_m\left(1 - e^{-kt}\right) \quad (1)$$

where, R_t is the recovery (%) at a time t (minutes), R_m is the maximum recovery (%), and k is the first-order rate constant (s^{-1}).

2.3. Batch flotation experiments

Around 500 g of the Pb/Zn complex sulfide ore was added to saline water of a certain concentration (1, 10, 100 and 500 mM NaCl) or seawater (ion composition in Table 1) and was ground at 50% solid/liquid ratio (% w/v) for 10 min using a rod mill. After milling, the pulp was transferred to a 3L laboratory flotation cell and agitated with the air valve turned off. The pH of the pulp was adjusted to 9 (±0.1) using NaOH. The pulp was then conditioned for 5 min before the air valve was turned on, to an air flow rate of 4 L/min, and a froth concentrate was collected for approximately 5 min. From each experiment, the collected froth concentrates and tailings were recovered, filtered, and dried. During filtering, the solid samples were rinsed with DI water to

eliminate any salt residue. Once dry, a small amount was removed from each concentrate and tailing for Pb and Zn assays. Each sub-sample was suspended in an aqua regia solution and digested using a hot plate for 1 h. Once digestion was completed, all samples were appropriately diluted and analysed for Pb and Zn using ICP-MS.

2.4. Zeta potential measurements

Dilute mixtures containing either 1 mM or 10 mM NaCl and ultrafine (~5 μm) lead or zinc sulfide particles were prepared prior to zeta potential measurements. The pH of each test solution was adjusted using HCl or NaOH, so that each solution sample had a different pH, in a range from pH 2 to pH 10. About 1 mL of each suspension was then transferred to a Malvern Dip Cell (Malvern Instruments Ltd., Malvern, UK). The dip cell was placed in a Malvern Nano-ZS90 zeta potential analyser (Malvern Instruments Ltd., Malvern, UK) and the zeta potential measurements were performed at room temperature. The measurements were repeated at least three times for each solution condition. The experimental zeta potentials for ZnS particles, conditioned in 10 mM NaCl solution, at pH values of 2–10, were used to calibrate the charge regulation parameters in the ZnS surface complexation model, described by Eq. (2–5).

2.5. Competitive adsorption of ions at the zinc sulfide surface sites

In our previous work, (Nowosielska et al., 2022), we presented a two-site/nonamphoteric surface complexation model for lead sufide (galena), which was successful at predicting the zeta potential behaviour of PbS particles. In this current work we aim at extending our investigation of the competitive ion adsorption on a metal sulfide surface by applying this same model to a system of negatively charged sulfur (S) sites and neutral/positively charged zinc (Zn) sites on a ZnS surface.

In general, our chemisorption model describes ion competition taking place at the neutral/positive and the negative surface sites within the metal sulfide lattice. The interactions at the negative surface sites are determined by the H^+ ions competing with cations (Na^+), as illustrated by Eq. (2–3):

$$XH \Leftrightarrow {}^{p}K_{H1} X^- + H^+ \tag{2}$$

$$XNa \Leftrightarrow {}^{p}K_{Na} X^- + Na^+ \tag{3}$$

while at the neutral sites, Eq. (4–5), H^+ ions are competing with anions (Cl^-), with the dissociation reactions expressed as:

$$XH^+ \Leftrightarrow {}^{p}K_{H2} X + H^+ \tag{4}$$

$$XCl^- \Leftrightarrow {}^{p}K_{Cl} X + Cl^- \tag{5}$$

Here the terms pK_{H1} and pK_{H2} are the equilibrium constants associated with the surface adsorption of protons. The equilibrium constants for the adsorption and desorption reactions of all ions were determined by least-square fitting to the measured zeta potential values for the different ionic concentrations.

The total surface charge (σ_s) for a given site can be calculated according to:

$$\sigma_s = q_s N_s + \sum_i q_i \Gamma_i \tag{6}$$

where, q_s is the charge of a dissociated site, N_s is the site density (number of sites per unit area) and q_i is the ionic charge (Parsons and Salis, 2019).

The total amount of bound charge (Γ_i) from ion i can be calculated from:

$$\Gamma_i = \frac{N_s}{A_s}\left[\frac{a_i}{K_i} + \sum_j a_i a_j \left(\frac{1}{K_i K_{ij}} + \frac{1}{K_j K_{ji}}\right)\right] \tag{7}$$

where, K_i and K_j represent a single adsorption of ions i and j, respectively. The terms K_{ij} and K_{ji} represent a double-binding of ion j to a site where ion i is already bound, and a double-binding of ion i to a site with ion j already bound. However, in the case of PbS and ZnS, the model describes nonamphoteric ion competition, meaning, it does not require double-binding constant terms K_{ij} and K_{ji} in the calculation. The parameters for an air bubble (Table 5) include the double-binding constant terms K_{ij} and K_{ji}, therefore, we present the full calculation sequence as Eq.(7).

A_s is a measure of the total association, and is the inverse of γ_s (γ_s being the fraction of fully dissociated surface sites), and can be written as:

$$A_s = \frac{1}{\gamma_s} = 1 + \sum_m \frac{a_m}{K_m}\left(1 + \sum_n \frac{a_n}{K_{mn}}\right) \tag{8}$$

The term a_i does not describe the surface activity of an ion, rather it corresponds to the "partial ion activity" at a particular concentration, and according to Parsons and Salis (2019), is quantified by:

$$a_i = c_i^{bulk} e^{-q_i \psi_0 / kT} \tag{9}$$

where, c_i^{bulk} is the concentration of ion i in the bulk, ψ_0 is the electrostatic potential at the surface, k is the Boltzmann constant (1.3806×10^{-23} J/K) and T is the temperature (298 K).

2.6. Total interaction free energy and the DLVO theory

The DLVO theory established by Derjagiun and Landau (1941) and Verwey and Overbeek (1948) describes colloidal stability between two objects based on an assumption that the attractive and repulsive interactions are independent and therefore can be added together at each interacting distance. The total interaction free energy (F_{tot}) which represents the sum of all the attractive and repulsive forces for any given system can be broken down into four individual components:

$$F_{tot} = F_{el} + F_{en} + F_{vdW} + F_{chem} \tag{10}$$

The term F_{el} represents the direct electrostatic energy due to surface and electrolyte charges and is calculated from the electrostatic potential $\psi(z)$ generated by physisorbed ions and by the surface charge (Eq. (6)) (Parsons and Ninham, 2012):

$$F_{el} = \frac{\varepsilon_0 \varepsilon}{2} \int_0^L \left(\frac{d\psi}{dz}\right)^2 dz \tag{11}$$

Here z represents the ion's distance from the surface and L represents the separation distance between the two interacting surfaces.

The term F_{en} in Eq. (10) is the contribution due to the ideal entropy (osmotic energy) of ions physisorbed near the surface. It is calculated from the concentration profiles $c_i(z)$ of the adsorbed ions, according to the following:

Table 5
Parameters used to fit the chemisorption model for an air bubble calibrated using the measured bubble zeta potentials in 10 mM NaCl, taken from Yang et al. (2001).

PARAMETER	VALUE
N_S(sites m^{-2})	4.676×10^{16}
pK_H	5.812
pK_{HH}	2.984
pK_{HCl}	1.962

$$F_{en} = kT\sum_{i}\int_{0}^{L} dz\left\{c_i(z)\ln\frac{c_i(z)}{c_{i0}} - c_i(z) + c_{i0}\right\} \quad (12)$$

where c_{i0} is the bulk activity of ion i (Parsons and Ninham, 2012).

The term F_{chem} represents the chemisorption free energy resulting from ion binding, also known as charge regulation. A detailed description of this energy component can be found in the studies of Parsons and Salis (2015) and (2019). In this study, the chemisorption free energy of an air bubble was calculated by applying a one-site/two pK surface complexation model for an air bubble, which was first introduced by Leroy et al. (2012).

The non-electrostatic van der Waals contributions (F_{vdW}) in Eq. (10) are characterised by a Hamaker constant (A_{132}) for the system with:

$$F_{vdW} = \frac{-A_{132}}{12\pi L^2} \quad (13)$$

where L represents the separation distance between the two interacting surfaces.

A Hamaker constant classifies the interaction between sphere (1) and sphere (2) immersed in aqueous medium (3). Using Lifshitz theory, the Hamaker constant can be calculated from the frequency dependent dielectric properties (optical spectra) of the continuous phases (Lee and Sigmund, 2002; Bergström, 1997). The non-retarded Hamaker constant (A_{132}) can be approximated as:

$$A_{132} = \frac{3kT}{2}\sum\nolimits'_{m=0}^{\infty}\sum_{s=1}^{\infty}\frac{(\Delta_{13}\Delta_{23})^s}{s^3} \quad (14)$$

The prime of the first summation indicates that the first term, when m = 0, is given half weight (ie. is multiplied by 0.5) (Takagishi et al., 2019).

The difference in the dielectric response function of materials k and l, Eq. (15), is represented by a reflection coefficient $\Delta_{kl}(i\xi_m)$, where i is the imaginery unit and ξ_m is the Matsubara frequency, according to the following:

$$\Delta_{kl(i\xi_m)} = \frac{\varepsilon_k(i\xi_m) - \varepsilon_l(i\xi_m)}{\varepsilon_k(i\xi_m) + \varepsilon_l(i\xi_m)} \quad (15)$$

From the Lifshitz theory, the Matsubara frequency (ξ_m) represents the imaginary frequency, which can be calculated by:

$$\xi_m = m\frac{4\pi^2 kT}{h} \quad (16)$$

Here h is the Planck constant (6.626×10^{-34} J/K), k is the Boltzmann constant, m is an integer number (0,1,2,3,4…) and T is the temperature. At room temperature, ξ_m are sampled at integral multiples of 2.4×10^{14} rad/s.

We apply a model for the dielectric function of lead and zinc sulfide provided by Bergström (1997), using:

$$\varepsilon(i\xi_m) = 1 + \frac{C_{UV}}{1 + \left(\frac{\xi_m}{\omega_{UV}}\right)^2} + \frac{C_{IR}}{1 + \left(\frac{\xi_m}{\omega_{IR}}\right)^2} \quad (17)$$

Optical parameters C_{UV} and C_{IR} are the adsorption strengths in the UV and IR range, and for a cubic PbS these are 15.04 and 153. For a hexagonal ZnS, the adsorption strengths in the UV and IR range are 4.153 and 3.55, respectively, while for a cubic ZnS, these values are 4.081 and 3.27, respectively. Similarly, the terms ω_{UV} and ω_{IR}, which represent the adsorption frequencies in the UV and IR range, are 0.167 (10^{16} rad/s) and 0.14 (10^{14} rad/s) for a cubic PbS, 1.04 (10^{16} rad/s) and 0.52 (10^{14} rad/s) for a hexagonal ZnS, and 0.939 (10^{16} rad/s) and 0.54 (10^{14} rad/s) for a cubic ZnS, respectively (Bergström, 1997). The Hamaker constants for the interactions presented in this study are listed in Table 6. These were calculated using dielectric data for water, taken from Fiedler et al. (2020).

The Debye length characterizes the screening distance of the electrostatic force, denoted as (κ^{-1}), and is defined as:

$$\kappa^{-1} = \sqrt{\frac{\varepsilon_r\varepsilon_0 kT}{e^2\sum_i \rho_i^{\infty} z_i^2}} \quad (18)$$

where, ε_0 is the permittivity of free space, ε_r is the dielectric constant of the medium, k is the Boltzmann constant, T is the temperature, e is the electronic charge, ρ_i is the number density of ion i and z_i is the ion valency. The calculated Debye lengths (κ^{-1}) for 1, 10 and 100 mM NaCl solutions were 9.62, 3.04 and 0.96 nm, respectively.

Table 6
The Hamaker constants (A_{132}) for the interactions in this study.

Interaction	(A_{132}) J
PbS (cubic) - water - PbS (cubic)	5.5693×10^{-20}
PbS (cubic) - water - Bubble	2.7741×10^{-21}
PbS (cubic) - water - ZnS (cubic)	2.3254×10^{-20}
ZnS (cubic) - water - ZnS (cubic)	5.0113×10^{-20}
ZnS (cubic) - water - Bubble	-3.3306×10^{-20}
ZnS (hexagonal) - water - Bubble	-4.0206×10^{-20}

2.6.1. The Poisson-Boltzmann model

The total interaction free energy described by Eq. (10) results from ion adsorption at the surface, in response to the electrostatic potential $\psi(z)$, where each ion forms a concentration profile $c_i(z)$. Assuming that each ion is in equilibrium with the bulk solution, the concentration profile $c_i(z)$ follows a Boltzmann distribution, determined by the electrostatic energy of the ion, according to:

$$c_i(z) = c_{i\infty}\exp\left(-\frac{z_i e\psi(z)}{kT}\right) \quad (19)$$

where k is the Boltzmann constant, T is the temperature and $c_{i\infty}$ is the bulk number concentration of all the ions.

The electrostatic potential $\psi(z)$ can be calculated using the Poisson equation:

$$\frac{d^2}{dz^2}\psi(z) = -\frac{e}{\varepsilon\varepsilon_0}\sum_i z_i c_{i\infty}\exp\left(-\frac{z_i e\psi(z)}{kT}\right) \quad (20)$$

where, e is the elementary charge and z_i is the valency of the corresponding ion. ε and ε_0 are the dielectric constant of the medium and the permittivity of free space. Solving for $c_i(z)$ and $\psi(z)$ simultaneously, Eq. (19) and Eq. (20) together, forms the nonlinear Poisson-Boltzmann (PB) model.

Prior to solving the Poisson equation Eq. (20), a set of boundary conditions need to be defined. These boundary conditions relate the gradient of the electrostatic potential at the surface of the interacting objects to their respective surface charges, as follows:

$$\left(\frac{d\psi}{dz}\right)_{surface} = \frac{-\sigma}{\varepsilon\varepsilon_0} \quad (21)$$

The charge regulation model, Eq. (6), is then applied to determine the surface charge of the two surfaces. We solved the nonlinear Poisson-Boltzmann (PB) model by finite element methods using the FEniCS software (Alnæs et al., 2015). Once $c_i(z)$ and $\psi(z)$ have been calculated, they are used to determine the total interaction free energy (Eq. (10)) between the two interacting objects, both represented as flat planes. The Derjaguin approximation (Derjaguin, 1934) is then applied to convert the flat-plane interaction energy (F_{tot}) from Eq. (10) into an interaction energy $E_S(L)$ between the two spherical surfaces:

$$E_S(L) = \pi\left(\frac{D_1 D_2}{D_1 + D_2}\right)\int_L^{\infty} dL' F_{tot}(L') \quad (22)$$

where, D_1 and D_2 are the diameters of sphere (1) and sphere (2), respectively and L is the separation distance (Chan et al., 1980).

Fig. 4 illustrates the sequence of steps required to perform the calculations.

1. Zeta potentials are measured as a function of pH and the ionic concentration.
2. The measured zeta potentials from Step 1 are used to calibrate the charge regulation parameters of our model, determining the charge-regulated surface charge (σ_s) in Eq. (6). The charge regulation parameters are fitted by least-square difference to minimize the difference between the measured zeta potentials and the surface potentials calculated by the PB model for zinc sulfide and air bubble surfaces, separately.
3. Using the charge regulation parameters from Step 2 and the PB model described by Eq. (19) and Eq. (20), the potential and the ion concentration profiles for zinc sulfide and an air bubble interacting at various separation distances (L) are calculated.
4. Using the electrostatic potentials and the ion concentration profiles calculated in Step 3, the total interaction free energy between the two surfaces, separated by a distance (L), is calculated using Eq. (10). The total free energy between two flat surfaces is then converted to a force between spherical particles using the Derjaguin approximation (Eq. (22)).

3. Results and discussion

3.1. Micro-flotation experiments

Fig. 5 shows the effects of NaCl concentration in solution on the recovery of lead sulfide during flotation.

The micro-flotation recovery (%) of lead sulfide (galena) as a function of NaCl concentration in solution has been reported in our previous study (Nowosielska et al., 2022), with the micro-flotation experiments carried out for a total of 7 min. For consistency between the PbS and ZnS micro-flotation experiments detailed in this study, the duration of our experiments has been extended to 10 min. From the results in Fig. 5, it can be seen that PbS recovery increased with increasing NaCl concentration in solution. At 10 min, the PbS recoveries (%) were 51.5%, 57.1% and 62.0% in the 1, 10 and 100 mM NaCl solutions, at pH 9 (±0.1), respectively. Here the increase in PbS recoveries can mainly be attributed to a shorter induction time as the solution ionic strength increases (Nguyen and Schulze, 2004). In addition, the compression of the ionic diffuse layers, resulting from an increase in NaCl concentration in solution, will have a positive effect on the particle-bubble interactions during flotation (Wang and Peng, 2014), resulting in higher mineral recovery.

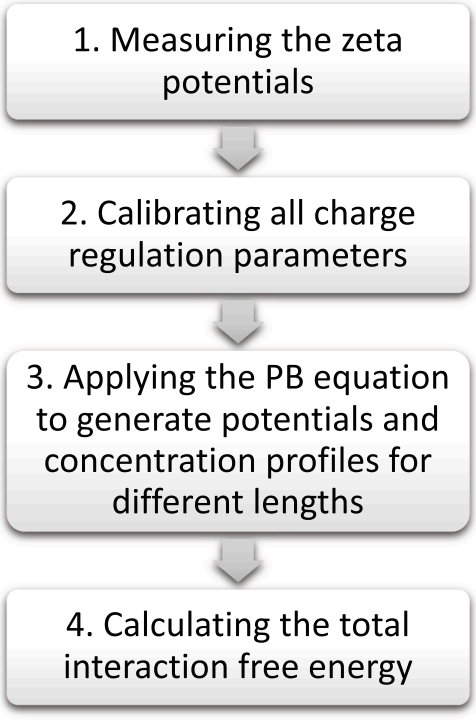

Fig. 4. The calculation/optimization sequence implemented in the study.

The effects of NaCl on the recovery of pure ZnS during flotation, as a function of the NaCl concentration in solution are shown in Fig. 6.

Fig. 6 shows that, similarly to PbS, ZnS recovery also increased with increasing NaCl concentrations. The highest recovery of around 67% after 10 min was reported for the test in 100 mM NaCl solution. Past studies attributed higher mineral recoveries to the changes in stability of the hydration layers in higher ionic strength in solution (Wang and Peng, 2014; October et al., 2020). It is well known that dissolved ions will alter the structure of water and, therefore, have an impact on mineral flotation. Monovalent ions (Na^+, Cl^-) have been shown to modify the structure of water, cause the compression of the double layers as well as control the surface activity of collectors. Past studies indicated that dissolved ions can either act as "structure makers" (small inorganic ions: Na^+, Cl^-, Li^+, F^-) or "structure breakers" (large inorganic ions: K^+, Cs^+, I^-) for water (Wang and Peng, 2014). Na^+ and Cl^- serve as structure makers for water, in their presence the water molecules will be strongly hydrogen bonded, therefore, the adsorption of a cationic or anionic collector at the hydrated surface will be difficult (Hancer et al., 2001). On the other hand, structure breaker ions will show a tendency to destroy the structure of water, which will create more favourable conditions for the adsorption of the collector (Ozdemir et al., 2011). Dissolved ions have been shown to alter solution viscosity, affecting the solid and gas dispersions as well as the bubble rise velocity (Desnoyers and Perron, 1972), important in mineral flotation. It has been shown that small ions with structure making tendencies (eg. Na^+, Cl^-), increase the solution viscosity. Increasing solution viscosity can lead to a lower particle-bubble collisions during minerals flotation. The presence of Na^+ and Cl^- ions will also influence the hydrogen ion conductance (Leberman and Soper, 1995), manifested by a reduction in solution pH.

Other studies documented that during mineral flotation, increasing salt concentration in solutions not only impacts the behaviour of mineral particles but also affects the air bubbles by inhibiting their coalescence (Craig et al., 1993a; 1993b; Wu et al., 2016; Zhang, 2020), and by helping to create smaller sized bubbles which consequently enhance foam stability. Additionally, Craig et al. (1993a and 1993b) found that bubble coalescence is not determined by a single effect of a cation or an anion, but rather by the combining effect of the pair of ions present. According to a study by Henry and Craig (2010), the correlation of Na^+ and Cl^- will inhibit bubble coalescence, through an increase in the Gibbs-Marangoni pressure which depends on the specific interfacial adsorption profile of both cation and anion (Duignan, 2021). Castro et al. (2013) reported that for higher salt concentrations in solution, this reduction in bubble size significantly improves particle-bubble attachment efficiency and contributes to a higher mineral recovery. Moreover, a reduction in bubble size leads to an overall increase in the number of bubbles (ie. a higher bubble surface area flux) (Liu et al., 2013; Di Feo et al., 2021), which can help to increase the number of potential particle-bubble attachments.

Using the results shown in Figs. 5 and 6, we characterised the flotation response by the maximum recovery at infinite flotation time (R_m) and a rate constant (k), calculated for lead sulfide and zinc sulfide, for each NaCl concentration in this study. These are presented in Table 7.

It can be seen from the results in Table 7 that both the maximum recoveries (R_m) and the rate constants (k) increased with an increase in NaCl concentration, for both mineral samples. As the NaCl concentration was increased from 1 mM to 100 mM, the flotation rate constant for

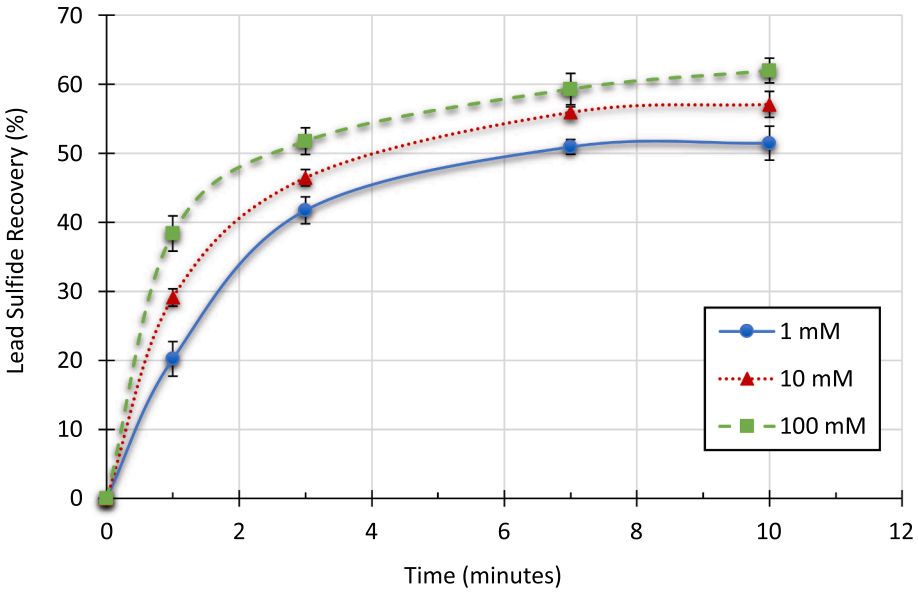

Fig. 5. Recovery of lead sulfide as a function of flotation time at different NaCl concentrations, at pH 9 (±0.1). Error bars indicate a standard error of the mean values.

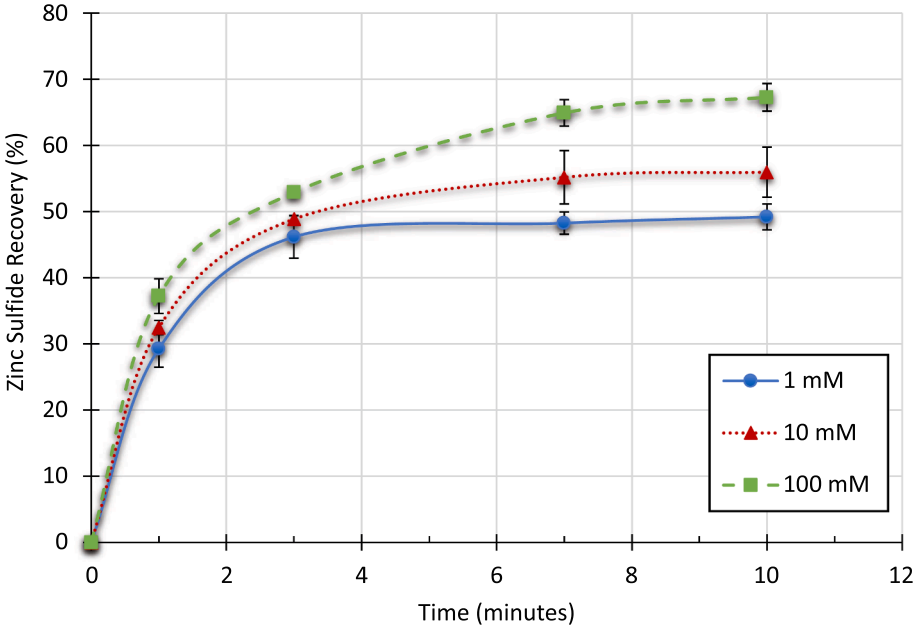

Fig. 6. Recovery of zinc sulfide, at pH 9 (±0.1), as a function of flotation time in different NaCl concentrations. Error bars indicate a standard error of the mean value.

Table 7
Fitting parameters (flotation rate constant k and maximum recovery R_m) used for calculating the kinetics (Klimpel's model) of the micro-flotation experiments in this study.

NaCl Concentration	Lead Sulfide		Zinc Sulfide	
	R_m (%)	k (s^{-1})	R_m (%)	k (s^{-1})
1 mM	53.5	5.48×10^{-3}	51.0	5.57×10^{-3}
10 mM	59.1	5.65×10^{-3}	58.0	5.61×10^{-3}
100 mM	64.0	5.77×10^{-3}	69.3	7.05×10^{-3}

PbS increased from 5.48×10^{-3} to 5.77×10^{-3} s^{-1}, and the maximum recovery increased from 53.5% to 64.0%. Similarly, when comparing the micro-flotation of ZnS in 1 and 100 mM NaCl concentrations in Fig. 6, the flotation rate constant increased from 5.57×10^{-3} to 7.05×10^{-3} s^{-1}, and the maximum recovery increased from 51.0% to 69.3%. It was interesting to note that for the highest NaCl concentration (100 mM), both the maximum recovery (R_{max}) and the rate constant (k) were larger for ZnS than PbS. Laskowski et al. (1991), documented that the flotation rate is influenced by the hydrophobicity of the particle. Based on the results in Table 7, we can assume that the hydrophobicity of our zinc sulfide sample was possibly slightly higher than our lead sulfide sample.

In a study by Fuerstenau et al. (1983), the authors reported that flotation rate (k) will be faster for higher salt concentrations since salt addition leads to a faster rupturing of the liquid film between particle and bubble. In a different study, Yoon and Sabey (1989) also indicated that flotation in highly concentrated electrolyte solutions introduced

faster flotation kinetics. Additionally, the faster flotation kinetics in the presence of higher NaCl concentrations have been attributed to the compression of the ionic diffuse layers, which facilitates particle-bubble adhesion (Wang and Peng, 2014). In one of their studies Marrucci and Nicodemo (1967) confirmed that the addition of salt to process water reduces bubble coalescence and in turn improves flotation kinetics. According to Pugh et al. (1997) the rate constant (k) can be controlled by controlling the aeration rate and/or the bubble size, where the latter has been found to be more effective. Our calculated rate constant values shown in Table 7 agree with previously reported findings, demonstrating that the addition of NaCl promotes faster mineral recoveries.

3.2. Batch flotation experiments

The lead sulfide and zinc sulfide recovery during the batch flotation experiments in solutions of different ionic strength (1, 10, 100 and 500 mM NaCl) and seawater (~510 mM NaCl) are illustrated in Fig. 7.

It is evident from the results in Fig. 7 that an increase in ionic strength of the process water results in higher mineral recoveries. The PbS recovery increased from around 9.7% in 1 mM NaCl to around 35.6% in 500 mM NaCl. Similarly, the recovery of ZnS in 1 mM NaCl solution was around 5.8% compared to around 21.7% in 500 mM NaCl solution. Past studies attributed these higher mineral recoveries at higher salt concentrations to a faster rupturing of the water film between a particle and bubble, leading to faster particle-bubble agglomerate formations, and higher flotation recoveries (Laskowski and Iskra, 1970; Laskowski and Castro, 2015; Jeldres et al., 2016). Additionally, higher mineral recoveries have been accredited to an increase in bubble stability (Biçak et al., 2012), a lower bubble coalescence (Craig et al., 1993a; 1993b), as well as to a reduction of bubble size (Calgaroto et al., 2014).

In Fig. 7, we noticed that the Pb and Zn recoveries in seawater (~510 mM NaCl), at pH 9 (±0.1), were lower than their recoveries in 500 mM NaCl concentration. The Pb recovery was around 28.3% and the Zn recovery was around 18.2%. According to Du et al. (2014), the drop in recovery may be attributed to the fact that various ions in seawater have different capabilities for changing the particle's physicochemical properties, surface charge or wettability, all of which will impact on mineral recovery. For example, the existence of Ca^{2+} ions in process water have been shown to significantly lower PbS recovery (Ikumapayi et al., 2012). Furthermore, SO_4^{2-} ions in seawater intensify passivation of a PbS surface, and in consequence decrease flotation recovery (Elizondo-Alvarez et al., 2017). A study by Parolis et al. (2008) showed that the depression of naturally floatable gangue was greater when divalent cations (Ca^{2+}, Mg^{2+}) were present compared to when monovalent cations (K^+, Na^+) were present.

According to Jeldres et al. (2016), some ionic species making up the composition in seawater may form colloidal precipitates at higher pH (pH 9 and above). Under basic pH conditions, chemical reactions in seawater may include the speciation of CO_2, Mg and Ca, as well as salt precipitation following these reactions:

$$CaCO_3 \leftrightarrow Ca^{2+} + CO_3^{2-} \quad (23)$$

$$MgCO_3 \leftrightarrow Mg^{2+} + CO_3^{2-} \quad (24)$$

$$Mg(OH)_2 \leftrightarrow Mg^{2+} + 2OH^- \quad (25)$$

Additionally, several studies have shown that the adsorption of hydroxy metal complexes on the mineral surface reduces particle hydrophobicity and depresses flotation (Laskowski and Castro, 2012).

The Pb and Zn assay grades (%) in concentrate, as a function of NaCl concentration in solution, at pH 9, are shown in Fig. 8.

The results from Fig. 8 indicate that the Pb and Zn assay grades are not significantly affected by the changes in NaCl concentration in solution. The concentrate recovered in 1 mM NaCl contained around 15% Pb and around 9.4% Zn, compared to around 15.2% Pb and around 9.7% Zn, in the 500 mM NaCl solution. Similarly, the Pb and Zn grades of the concentrate recovered in seawater contained around 15.2% Pb and around 10.1% Zn.

Fig. 9 shows the solid and water recoveries in the concentrate, for the batch flotation experiments using waters with different NaCl concentrations as well as seawater.

Fig. 9 shows the fraction of water recovered in the concentrate increased with an increasing NaCl concentration in solution. In 1 mM NaCl, water recovery was at around 90.2%, compared to around 95.2% in the 500 mM NaCl solution. Flotation experiments using seawater resulted in the highest water recovery of around 95.6%. Previous studies have shown that experiments using waters of higher ionic strength will generate higher water recoveries in the flotation concentrate (Corin et al., 2011; Corin and Wiese, 2014), which is what we see in Fig. 9. In a study by Cho and Laskowski (2002) the authors proposed that a decreased bubble coalescence at higher ionic strengths causes a reduction in the gas hold-up in the froth phase, which in turn allows for more water in the concentrate. Furthermore, these higher water recoveries could be assigned to an increase in bubble interfacial area and an increase in water–gas binding forces Cho and Laskowski, 2002. Manono

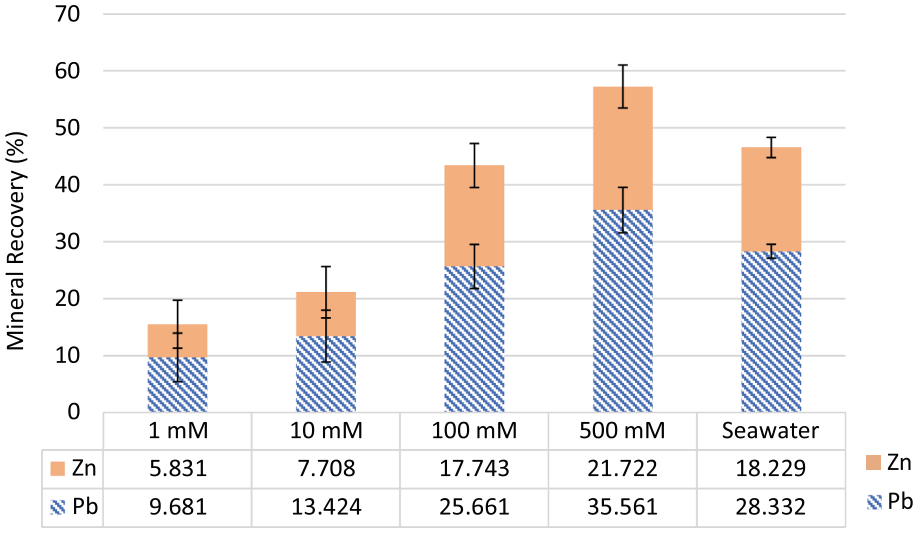

Fig. 7. Recovery of PbS and ZnS, as a function of NaCl concentration in solution (0, 1, 10, 100 and 500 mM NaCl) and seawater (~510 mM NaCl), at pH 9 (±0.1). Error bars indicate a standard error of the mean values.

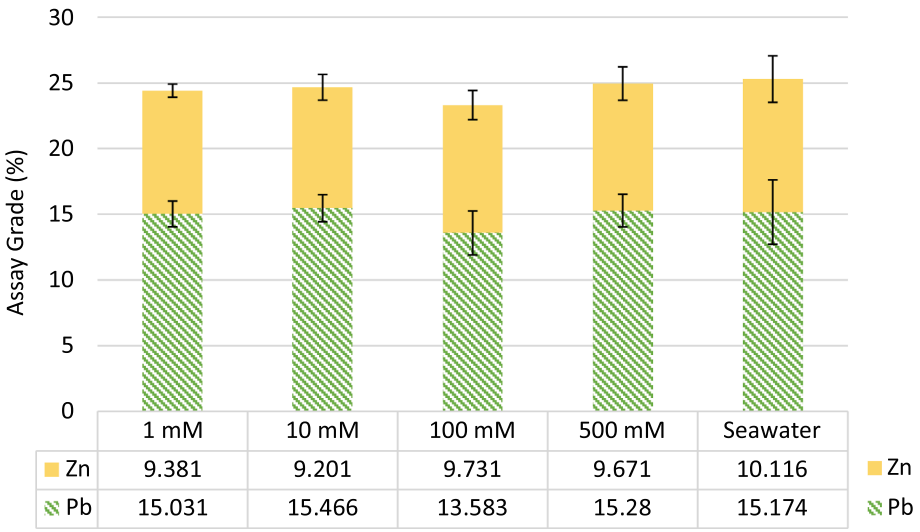

Fig. 8. The Pb and Zn assay grades (%) recovered in the flotation concentrates, as a function of NaCl concentration in solution (0, 1, 10, 100, 500 mM NaCl) and seawater (~510 mM NaCl), at pH 9. Error bars indicate a standard error of the mean values.

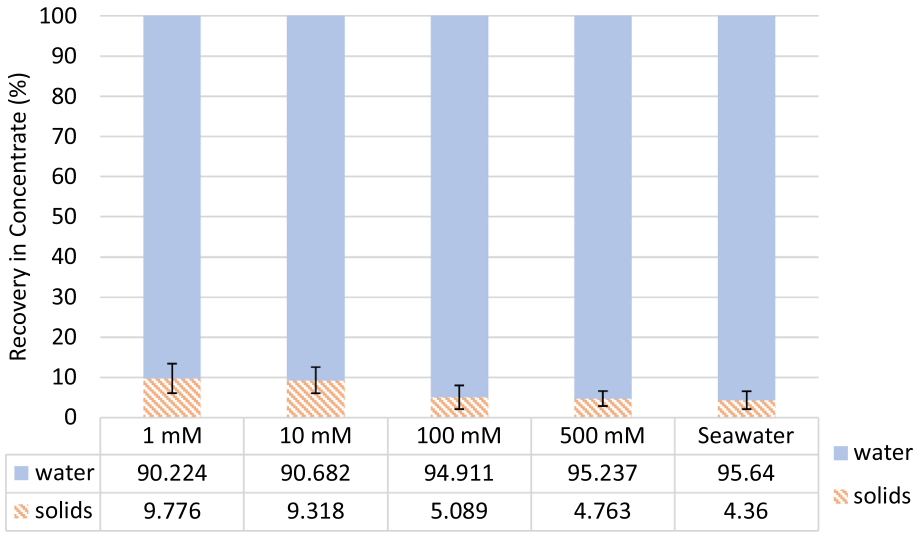

Fig. 9. The solids and water recoveries in the concentrate, as a function of NaCl concentration in solution (0, 1, 10, 100, 500 mM NaCl) and seawater (~510 mM NaCl), at pH 9. Error bars indicate a standard error of the mean values.

and Corin (2022) argued that the presence of divalent cations (Ca^{2+}, Mg^{2+}) and divalent anion (SO_4^{2-}) in the process water further increases water recoveries in the concentrate, which is what we notice in the case of seawater from Fig. 9.

3.3. *Zeta potential measurements and a chemisorption model for zinc sulfide*

The calculated zeta potential versus pH curves for zinc sulfide particles are shown in Fig. 10, with the values of the best-fit parameters presented in Table 4. For comparison, we also present the experimental zeta potential values for zinc sulfide particles, measured in 1, 5 and 10 mM NaCl solutions.

It is evident from Fig. 10 that the surface of zinc sulfide particles is positively charged in the acidic pH range and becomes increasingly negatively charged in the alkaline range, above the isoelectric point (IEP). The isoelectric point lies between pH 5.5–7, which is consistent with the previously reported IEP values for zinc sulfide particles (Muster et al., 1996). Past studies reported that the value of the IEP can reflect the level of sulfide mineral oxidation, where a low IEP indicates a non-oxidised surface (Fullston et al., 1999; Fairthorne et al., 1998). In a study by Williams and Labib (1985), the authors found that between pH 2–12, the ZnS zeta potential profile can be divided into two distinctive and relatively independent regions. The positive zeta potential region at low pH can be attributed to the adsorption of H^+ and Na^+ ions in saline water to the sulfur-rich sites on the surface of ZnS, according to Eq.(2–3). An excess number of cations on its surface will consequently give rise to a positively charged ZnS particle at low pH. An increase in the negative charge at higher pH can be explained by a stronger chemisorption of Cl^- ions on the positively charged metal-rich sites on the surface of ZnS, described by Eq.(5). Additionally, at higher pH values, the dissolution of H^+ ions from the surface into the solution, will result in the ZnS surface acquiring a negative charge.

The results from Fig. 10 suggest that an increase in NaCl concentration from 1 to 10 mM reduces the magnitude of the zeta potential while the chemisorption of salt ions results in displacement of the isoelectric point. This reduction in the magnitude of the zeta potential accompanies a decrease in the electrolytic repulsion between the two interacting surfaces (October et al., 2020 and 2021), due to a compression of the ionic diffuse layers at higher ionic concentrations

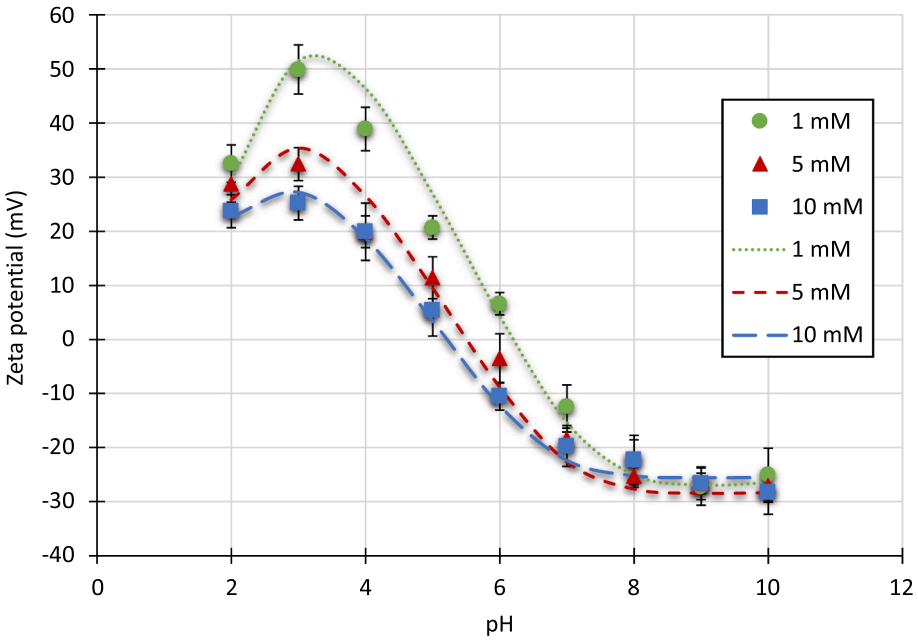

Fig. 10. Zeta potential versus pH curves for zinc sulfide particles conditioned in 1, 5 and 10 mM NaCl solutions. The error bars represent the standard error of the mean. Lines represent the chemisorption model from Eq. (2–5) predictions using the optimized parameters from Table 4.

(Moignard et al., 1977). When the potential on the particle surface approaches 0 mV, a weaker electrostatic repulsion will facilitate the formation of closely arranged particle networks at the liquid–air interfaces, in turn increasing the number of particles being carried by a single bubble (Huo et al., 2019). Several experimental studies have found that the maximum mineral recoveries were achieved at lower particle zeta potentials (Fuerstenau et al., 1983; Yoon and Sabey, 1989).

Shown in Fig. 10, ZnS zeta potentials calculated using our chemisorption model, Eq. (2–5), are in good agreement with the measured zeta potential values for the different NaCl concentrations and a broad range of pH. This provides confidence that the model is effective in predicting the zeta potential behaviour due to changes in pH and solution ionic strength.

Fig. 11 illustrates the zeta potential values for lead sulfide, zinc sulfide and air bubbles, measured in 10 mM NaCl background electrolyte solution, against pH values between 2 and 10.

The experimental zeta potential of lead sulfide, measured in 10 mM NaCl solution, show a negatively charged surface over the entire pH range, decreasing from around −14 mV at pH 2 to around −31 mV at pH 10. Studies have shown that a non-oxidised lead sufide surface will carry a negative charge, with the zeta potential values close to that of elemental sulfur (IEP < pH 1) (Fornasiero et al., 1993; Nowosielska et al., 2022). However, the zeta potentials of zinc sulfide indicated a positively charged surface from around + 24 mV to + 5 mV for pH values of less than 5, becoming more negative in the pH region > 6. At pH 9 (the pH chosen to carry out the experimental work), the difference

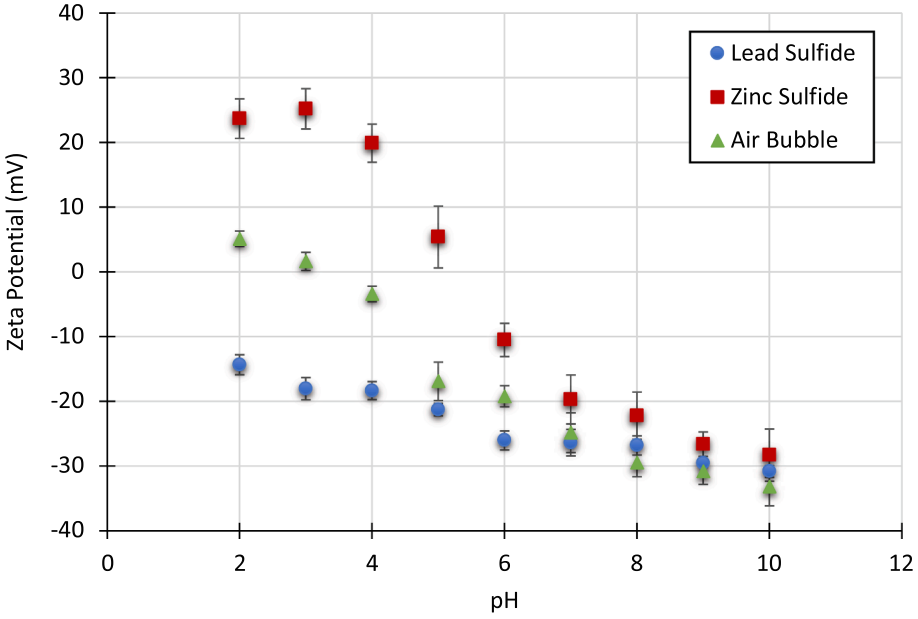

Fig. 11. Zeta potential of lead sulfide, zinc sulfide and an air bubble conditioned in 10 mM NaCl solution, as a function of solution pH. Error bars indicate a standard error of the mean values. The measured zeta potentials of an air bubble were taken from Yang et al. (2001).

between lead sulfide and zinc sulfide zeta potentials is reasonably small, which might imply a lower electrostatic attraction between the two mineral samples at this pH.

In 10 mM NaCl solution, at pH 9, an air bubble carries a negative charge with a zeta potential of around −31 mV. Our experiments were conducted at pH 9, where both mineral particles (lead sulfide and zinc sulfide) zeta potentials are less negative (-29.5 mV and −26.6 mV, respectively) than a bubble's zeta potential. According to Pugh et al. (1997), at these conditions, some hydrophobic coagulation could be taking place. Most likely, this hydrophobic coagulation is initiated by particle bridging by gas nuclei taking place during the entrapment of air bubbles by hydrophobic particles (Pugh et al., 1997).

3.4. Total interaction free energy

The total interaction free energy calculated using Eq. (10), representing the interactions of a cubic PbS and a hexagonal ZnS particle with an air bubble, as a function of NaCl concentration in solution, at pH 9, is shown in Fig. 12.

As can be seen in Fig. 12, in 1 and 10 mM NaCl concentrations, the total interaction energy between a sulfide (lead or zinc) particle and an air bubble was positive (repulsive) over the whole separation distance. On the principles of the DLVO theory, in 1 mM NaCl we expect to see particle-bubble interactions which are dominated by long-range repulsions, originating from stronger ion adsorptions at the surface. Consequently, particle-bubble attachment efficiency decreases in lower NaCl concentration. The results from our micro-flotation experiments support these predictions, showing lower PbS and ZnS recoveries in 1 mM NaCl solution.

Energy curves representing the particle-bubble interactions in 10 mM NaCl solution indicate lower repulsion with a decrease in height of the energy barriers. The calculated energy barriers are 0.16×10^{-15} J and 1.78×10^{-15} J, for the PbS-bubble and the ZnS-bubble interactions, respectively. In 100 mM NaCl concentration, the energy barrier for the PbS-bubble interaction disappears completely, as the interaction becomes solely controlled by the attractive van der Waals forces. Generally, an increase in NaCl concentration in solution shortens the screening distance, meaning less kinetic energy will be required for the PbS particle and bubble to form an attachment. This in turn should give rise to a higher mineral recovery, as seen in Fig. 5.

By contrast, the ZnS-bubble interaction in 100 mM NaCl is still largely controlled by forces of repulsion, with an energy barrier of around 1.45×10^{-15} J. The repulsive nature of the ZnS-bubble interactions has to do with the fact that the calculated Hamaker constants for the ZnS (cubic and hexagonal)-water-bubble interactions had negative values of -3.3306×10^{-20} J and -4.0206×10^{-20} J, respectively. In an asymmetric system where the aqueous medium (3) possesses dielectric properties intermediate between the dielectric properties for the different materials represented as sphere (1) and sphere (2), a negative Hamaker constant indicates a repulsive electrodynamic interaction between the materials, which gives rise to a less common repulsive behaviour of the van der Waals forces for this system (Bergström, 1997). In Fig. 6, however, the micro-flotation experiments clearly show that the ZnS particles did form aggregates with the air bubbles despite van der Waals forces contributing additional repulsion to the total interaction energy. This suggests the existence of some additional attractive interaction energy which counterbalances this repulsion. It might be possible that an additional attraction arises from the long-range nature of the hydrophobic effect when naturally hydrophobic particles are involved. Since this hydrophobic attraction will be much stronger than the van der Waals interaction, it is likely that as the Debye length approaches the decay length of the hydrophobic interaction, the energy barrier can be exceeded, and at that point, coagulation will begin (Pugh et al., 1997).

The next figures (Figs. 13-15) illustrate the theoretically predicted energies, describing the particle–particle and particle-bubble interactions during Pb/Zn complex sulfide ore flotation in NaCl solutions. Here we have chosen to compare the 10 mM and 500 mM NaCl concentrations, the latter simulating the NaCl concentration in seawater. To determine the level of heterocoagulation in the system, we first calculated the total interaction free energy versus separation distance (L) between a cubic PbS and a cubic ZnS particle, as a function of NaCl concentration in solution. The results are shown in Fig. 13.

The energy curve representing the PbS-ZnS interaction in 10 mM

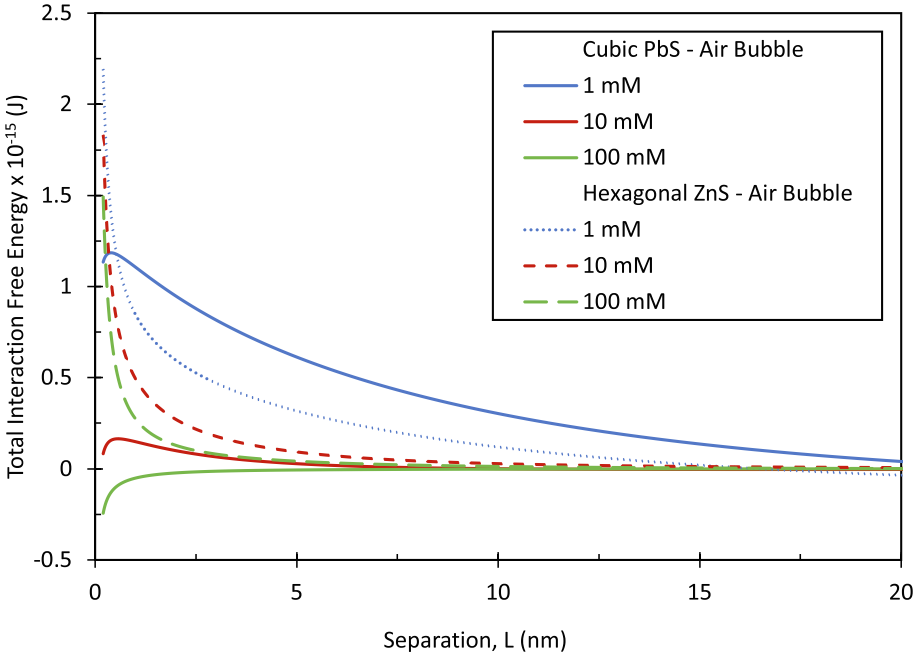

Fig. 12. The total interaction free energy versus separation distance (L) between a PbS (cubic)particle and an air bubble (solid lines), and between a ZnS (hexagonal) particle and an air bubble (broken lines), as function of NaCl concentration in solution, at pH 9. The diameters representing the size of the PbS and ZnS particles used in the calculations were 80 and 95.8 μm, respectively. The mean diameter of an air bubble was assumed to have a size of 2000 μm.

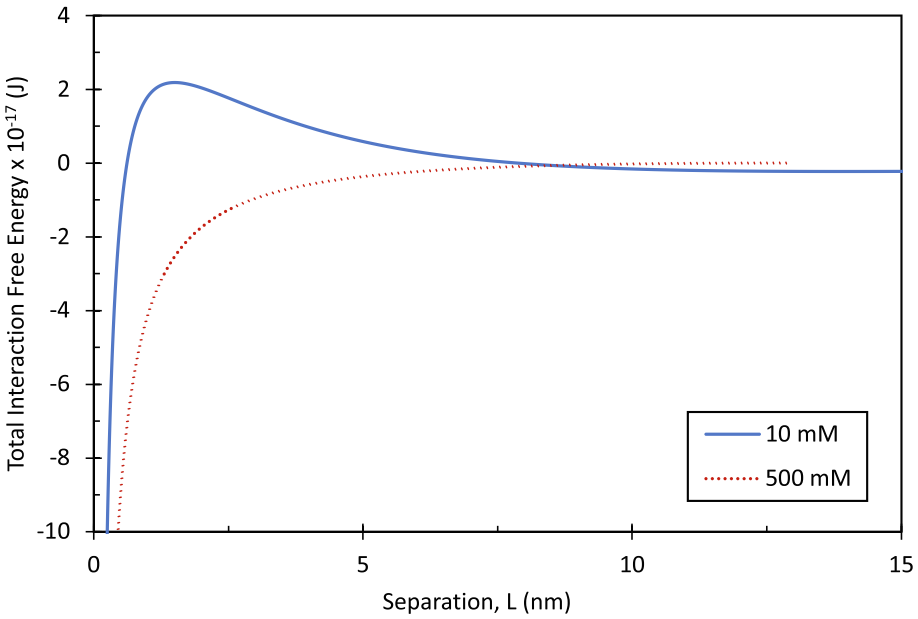

Fig. 13. The total interaction free energy vs separation distance (L), between a cubic PbS and a cubic ZnS particle, as a function of NaCl concentration in solution (10 and 500 mM), at pH 9. The mean particle diameter used in the calculations was 50.48 μm.

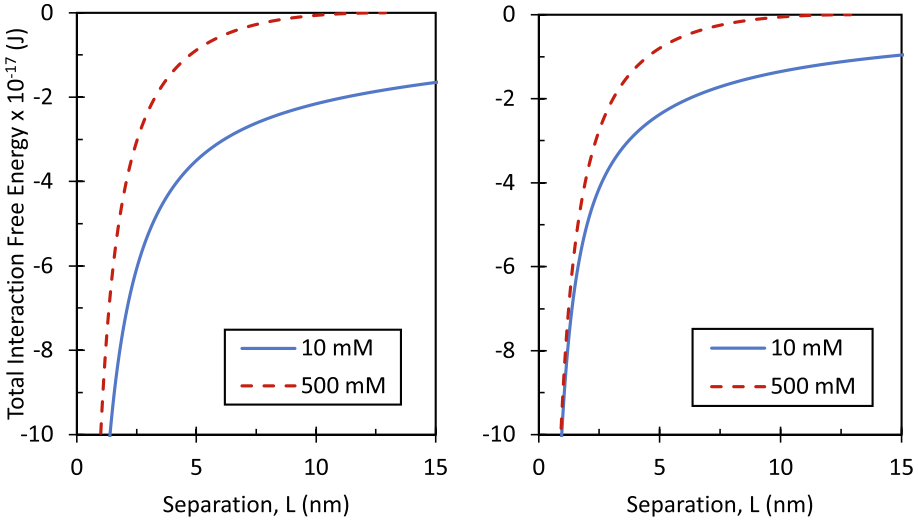

Fig. 14. The total interaction free energy vs separation distance (L) between two cubic PbS particles (left), and two cubic ZnS particles (right), as a function of NaCl concentration (10 and 500 mM), at pH 9. 50.48 μm was used as the mean diameter of the particles.

NaCl shows an energy barrier of around 2.2×10^{-17} J at around 1.5 nm separation distance. From the zeta potential measurements in Fig. 11, at pH 9, both PbS and ZnS particles carry a negative charge of around −30 mV. As these two particles begin to approach one another, their overlapping ionic diffuse layers will cause an imbalance in the charge distribution within the layers, resulting in the rise of an electrostatic repulsive energy between the two interacting particles, and hence the rise of an energy barrier. However, given enough time and kinetic energy, even electrostatically stabilized colloids with a relatively high energy barrier, will eventually agglomerate at the energy minimum found at small separation distances, which is what we see in the 10 mM NaCl energy curve in Fig. 13.

As expected, the calculated PbS-ZnS energy curve in 500 mM NaCl shows no repulsive electrostatic (ionic) contributions to the total interaction energy, with van der Waals forces responsible for the entire PbS-ZnS attraction. In terms of our flotation recoveries in 500 mM NaCl, due to this stronger attraction we can anticipate a higher particle coagulation in the pulp. Consequently, we end up with a mixed Pb and Zn recovery in the froth. With the design of our batch flotation experiments in this study, the fact that both, Pb and Zn, can be recovered simultaneously into a single concentrate is positive, considering that the presence of Pb^{2+} ions in the pulp has been shown to directly promote ZnS flotation (Morey et al., 2001). As seen in Fig. 13, at higher NaCl concentration of 500 mM the interaction between PbS and ZnS particles becomes attractive. Therefore, it may be possible that the recovery of ZnS particles is facilitated by the presence of PbS particles and mainly controlled by the attraction between the two minerals at higher NaCl concentrations. This way, the ZnS particles can be carried up and recovered in the froth, despite indicating a strong repulsion towards air bubbles (Fig. 15, right). On the other hand, the PbS particles can easily aggregate with the air bubbles due to a stronger PbS-air bubble attraction at higher NaCl concentrations, as shown in Fig. 15 (left).

Fig. 14 illustrates the total interaction free energy for the symmetrical systems of our study – for the two PbS particles (left), and for the

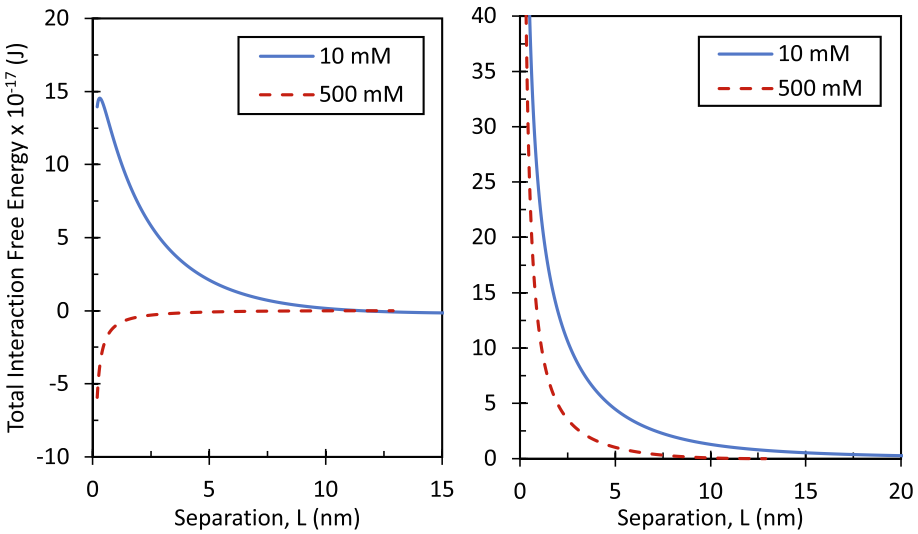

Fig. 15. The total interaction free energy vs separation distance (L) between a cubic PbS particle and an air bubble (left), and a cubic ZnS particle and an air bubble (right), as a function of NaCl concentration in solution (10 and 500 mM), at pH 9. 50.48 μm and 2000 μm were used as the mean particle and air bubble diameters, respectively.

two ZnS particles (right), versus separation distance (L), as a function of NaCl concentration in solution, at pH 9.

The energy curves representing PbS-PbS interactions (Fig. 14, left), show a dominating attraction over the whole separation distance (L), regardless of the NaCl concentration. The energy curve for the ZnS-ZnS interaction (Fig. 14, right) also indicates attraction at both NaCl concentrations considered. According to the DLVO theory, we know that in 500 mM NaCl, the screening of the electrostatic (ionic) repulsive energy results in interactions solely controlled by the van der Waals attractions. The calculated Hamaker constant values for the PbS(cubic)-water-PbS (cubic) and the ZnS(cubic)-water-ZnS(cubic) interactions, namely 5.5693×10^{-20} J and 5.0113×10^{-20} J, are similar to one another, meaning in 500 mM NaCl, they will generate nearly identical energy curves for both symmetrical interactions, as seen in Fig. 14.

In Fig. 14 (left and right), the attraction in the lower salt concentration (10 mM NaCl) is most likely attributed to a suppression of the electrostatic (ionic) contributions. The adsorption of cations (Na^+) via electrostatic attraction on the negatively charged ZnS surface site has the ability to neutralise/lower the ZnS particle surface charge. Therefore, a stronger attraction could be the result of interactions between particles which start to behave as if they do not have an electrical charge.

Fig. 15 illustrates the total interaction free energy for the mineral particle interactions with an air bubble, namely a cubic PbS particle (left), and a cubic ZnS particle (right), versus the separation distance (L), in 10 and 500 mM NaCl solutions, at pH 9.

Fig. 15 (left and right) shows that the PbS-bubble and ZnS-bubble interactions in 10 mM NaCl concentrations are dominated by repulsions. The PbS-bubble interaction has an energy barrier of around 15×10^{-17} J. In contrast, the PbS-bubble energy curve in 500 mM NaCl is solely controlled by the attractive van der Waals forces. Based on the results in Fig. 15 (left), PbS-bubble attachment will be easier in a higher NaCl concentration. The results from our experimental work (Figs. 5 and 7) support this prediction.

On the other hand, the ZnS-bubble interactions are all repulsive, irrespective of the increasing ionic strength in solution. The overall repulsion, however, is slightly lower in 500 mM compared to 10 mM NaCl. The fact that a significantly high repulsion controls the ZnS-bubble interactions even at a higher (500 mM) NaCl concentration can mainly be attributed to a repulsive nature of the van der Waals interactions, characterised here by a negative Hamaker constant value.

The analysis of the energy curves in Fig. 15 leads to a conclusion that the air bubbles will more likely and easily form aggregates with PbS particles than with ZnS particles. Possibly this could be one of the reasons why we see higher PbS recoveries compared to the ZnS recoveries during our batch flotation experiments (Fig. 7). Nevertheless, our results did show that zinc sulfide particles and bubbles were able to overcome the energy barriers and form stable aggregates even in the lowest (1 mM) NaCl concentration, despite a repulsive nature of the van der Waals forces. Due to the intense turbulence inside a flotation cell, it may be possible that the particles and bubbles can achieve the required velocities for many particle-bubble collisions, and if they can withstand these turbulent conditions, stable particle-bubble aggregates will be recovered in the froth.

4. Conclusion

In this study we have investigated the effects of water salinity on lead and zinc sulfide flotation. We performed separate micro-flotation experiments using pure PbS and ZnS mineral samples in 1, 10 and 100 mM NaCl solutions, to gain a better understanding of the effects of NaCl on the individual Pb and Zn recoveries. The results indicated that increasing NaCl concentration in solution improves the recovery of both mineral samples. Using the results from our micro-flotation experiments, we were able to calculate the first-order flotation rate constants as well as the maximum recoveries for each test condition. A faster flotation rate was reported for solutions of higher ionic strength, which was attributed to a faster particle-bubble adhesion when the ionic diffuse layers compress. Additionally, in this study we carried out batch flotation experiments on a Pb/Zn complex sulfide ore, using 1, 10, 100 and 500 mM NaCl solutions, as well as seawater. The outcome of these experiments showed: a) increasing Pb and Zn recoveries in increasing NaCl concentrations which can be attributed to lower zeta potentials due to the compression of the ionic diffuse layers, creation of smaller-sized bubbles and inhibition of bubble coalescence; b) in the case of seawater, the overall Pb and Zn recoveries decreased, which can be related to negative effects of different ions (e.g. Ca^{2+}, Mg^{2+}, SO_4^{2-}) present in the seawater on mineral recovery; c) Pb and Zn assay grades were not affected by changes in NaCl concentration in solution; and d) water recovery (%) in the concentrate was higher for higher NaCl concentrations.

Electrokinetic measurements were conducted on both mineral samples, with the ZnS zeta potential values being used to optimise the parameters in our ZnS chemisorption model. The calculated zeta potentials

proved to be a good match to our experimental zeta potential values, indicating that this model can be effectively implemented for predicting the zeta potential behaviour for other pH and NaCl concentrations.

Also included in this study were calculations of particle–particle and particle-bubble total interaction free energies versus separation distance, for the different NaCl concentrations. In summary; a) repulsion dominated asymmetric particle–particle interactions in lower NaCl concentrations; b) at higher NaCl concentrations, repulsion no longer controlled asymmetric particle–particle interactions; c) the symmetric particle–particle interactions were independent of any changes in NaCl concentration, and were always controlled by stronger attractive forces; d) at higher NaCl concentrations in solution, the interaction between PbS and an air bubble indicated attraction, while the ZnS-bubble interactions were always repulsive, despite an increase in ionic strength; e) these ZnS-bubble repulsions were attributed to a repulsive nature of the van der Waals forces, due to a negative Hamaker constant calculated for the ZnS-bubble interaction in water.

The focus of this study was to investigate the effects of salinity on the recovery of lead and zinc sulfide via flotation. Future studies will incorporate these findings and further examine the effects of salinity on the flotation of a complex Pb/Zn sulfide ore, in the presence of some common flotation reagents.

CRediT authorship contribution statement

Anna M. Nowosielska: Conceptualization, Methodology, Validation, Formal analysis, Investigation, Writing – original draft, Visualization. **Aleksandar N. Nikoloski:** Conceptualization, Methodology, Resources, Writing – review & editing, Supervision, Funding acquisition. **Drew F. Parsons:** Conceptualization, Methodology, Software, Writing – review & editing, Supervision.

Declaration of Competing Interest

The authors declare that they have no known competing financial interests or personal relationships that could have appeared to influence the work reported in this paper.

Data availability

Data will be made available on request.

References

Alnæs, M., Blechta, J., Hake, J., Johansson, A., Kehlet, B., Logg, A., Richardson, C., Ring, J., Rognes, M.E. and Wells, G.N. (2015). The FEniCS Project Version 1.5. Archive of Numerical Software, Vol.3 No.100.

Bergström, L., 1997. Hamaker constants of inorganic materials. Adv. Colloid Interface Sci. 70, 125–169.

Biçak, Ö., Ekmekçi, Z., Can, M., Öztürk, Y., 2012. The effect of water chemistry on froth stability and surface chemistry of the flotation of a Cu-Zn sulfide ore. Int. J. Miner. Process. 102-103, 32–37.

Blake, T.D., Kitchener, J.A., 1973. Stability of aqueous films on hydrophobic methylated silica. J. Chem. Soc. 68, 1435–1442.

Calgaroto, S., Wilber, K.Q., Rubio, J., 2014. On the nanobubbles interfacial properties and future applications in flotation. Miner. Eng. 60, 33–40.

Castro, S., Miranda, C., Toledo, P., Laskowski, J.S., 2013. Effects of frothers on bubble coalescence and foaming in electrolyte solutions and seawater. Int. J. Miner. Process. 124, 8–14.

Chan, D., Pashley, R., White, L., 1980. A simple algorithm for the calculation of the electrostatic repulsion between identical charged surfaces in electrolyte. J. Colloid Interface Sci. 70 (1), 283–285.

Cho, Y.S., Laskowski, J.S., 2002. Effect of flotation frothers on bubble size and foam stability. Int. J. Miner. Process. 64 (2-3), 69–80.

Corin, K.C., Wiese, J.G., 2014. Investigating froth stability: a comparative study of ionic strength and frother dosage. Miner. Eng. 66, 130–134.

Corin, K.C., Reddy, A., Miyen, L., Wiese, J.G., Harris, P.J., 2011. The effect of ionic strength of plant water on valuable mineral and gangue recovery in a platinum bearing ore from the Marensky Reef. Miner. Eng. 24, 131–137.

Craig, V.S.J., Ninham, B.W., Pashley, R.M., 1993a. Effect of electrolytes on bubble coalescence. Nature 364 (6435), 317–319.

Craig, V.S.J., Ninham, B.W., Pashley, R.M., 1993b. The effect of electrolytes on bubble coalescence in water. J. Phys. Chem. 97 (39), 10192–10197.

Dai, Z., Fornasiero, D., Ralston, J., 2000. Particle-bubble collision models- A review. Adv. Colloid Interface Sci. 85 (2-3), 231–256.

Desnoyers, J.E., Perron, G., 1972. The viscosity of aqueous solutions of alkali and tetraalkylammonium halides at 25°C. J. Solution Chem. 1 (3), 199–212.

Derjagiun, B.V., Landau, L., 1941. The theory of stability of strongly charged lyophobic sols and of adhesion of strongly charged particles in solution of electrolytes. Acta Physochim. USSR 14, 633–662.

Derjaguin, B., 1934. Untersuchungen über die Reibung und Adhäsion. IV. Kolloid-Zeitschrift 69 (2), 155–164.

Di Feo, A., Hill-Svehla, C.M., Hart, B.R., Volchek, K., Morin, L., Demers, A., 2021. The effects of water recycling on flotation at North American concentrator. Miner. Eng. 170, 107037.

Du, H., Ozdemir, O., Wang, X., Cheng, F., Celik, M.S., Miller, J.D., 2014. Flotation chemistry of soluble salts minerals: from ion hydration to colloid adsorption. Mining, Metallurgy and Exploration 31, 1–20.

Duignan, T.T., 2021. The surface potential explains ion specific bubble coalescence inhibition. J. Colloid Interface Sci. 600, 338–343.

Elizondo-Alvarez, M.A., Flores-Alvarez, J.M., Davila-Pulido, G.I., Uribe-Salas, A., 2017. Interaction mechanism between galena and calcium and sulfate ions. Miner. Eng. 111, 116–123.

Fairthorne, G., Brinen, J.S., Fornasiero, D., Nagaraj, D.R., Ralston, J., 1998. Spectroscopic and Electrokinetic study of the adsorption of butyl ethoxycarbonyl thiourea on chalcopyrite. Int. J. Miner. Process. 54 (3-4), 147–163.

Fiedler, J., Boström, M., Persson, C., Brevik, I., Corkery, R., Buhmann, S.Y., Parsons, D.F., 2020. Full-spectrum high-resolution modelling of the dielectric function of water. J. Phys. Chem. B 124 (15), 3103–3113.

Fornasiero, D., Li, F., Ralston, J., 1993. Oxidation of galena II. Electrokinetic Study. J. Colloid Interface Sci. 164, 345–354.

Fuerstenau, D.W., Rosenbaum, J.M., Laskowski, J., 1983. Effect of surface functional groups on the flotation of coal. Colloid and Surfaces 8 (2), 153–173.

Fuerstenau, M.C., Jameson, G.J., Yoon, R.-H., 2007. Froth flotation: A century of innovation. Society of Mining, Metallurgy and Exploration.

Fullston, D., Fornasiero, D., Ralston, J., 1999. Zeta potential study of the oxidation of copper sulfide minerals. Colloid Surf. A: Physicochem. Eng. Aspects 146 (1–3), 113–121.

Hancer, M., Celik, M.S., Miller, J.D., 2001. The significance of interfacial water structure in soluble salt flotation systems. J. Colloid Interface Sci. 235 (1), 150–161.

Henry, C.L., Craig, V.S.J., 2010. The link between ion specific bubble coalescence and Hofmeister effects is the partitioning of ions within the interface. Langmuir 26 (9), 6478–6483.

Huang, B.o., Lai, H., Deng, J., Xu, H., Fan, G., 2019. Study on the interaction between Galena and Sphalerite during grinding based on the migration of surface components. ACS Omega 4 (7), 12489–12497.

Huo, W., Zhang, X., Gan, K.e., Chen, Y., Xu, J., Yang, J., 2019. Effect of zeta potential on properties of foamed colloidal suspension. Journal of European Ceramic Society 39 (2-3), 574–583.

Ikumapayi, F., Makitalo, M., Johansson, B., Rao, K.H., 2012. Recycling of process water in sulphide flotation: effect of calcium and sulphate ions on flotation of galena. Miner. Eng. 39, 77–88.

Jeldres, R.I., Forbes, L., Cisternas, L.A., 2016. Effect of Seawater on Sulfide Ore Flotation: A review. Miner. Process. Extr. Metall. Rev. 37 (6), 369–384.

Klassen, V.I., Mokrousov, V.A., 1963. An introduction to the theory of flotation. Butterworths, London.

Laskowski, J.S., Castro, S., 2012. Hydrolizing ions in flotation circuits: seawater flotation. XIII International Minerals Processing Symposium, Bodrum, Turkey.

Laskowski, J.S., Castro, S., 2015. Flotation in highly concentrated electrolyte solutions. Int. J. Miner. Process. 144, 50–55.

Laskowski, J.S., Iskra, J., 1970. Role of capillary effects in bubble-particle collision in flotation. Trans. Inst. Min. Metall. 79, 6.

Laskowski, J.S., Xu, Z., Yoon, R.H., 1991. The energy barrier in particle to bubble attachment and its effect on flotation kinetics. XVII International Minerals Processing Congress, Dresden, Germany.

Leberman, R., Soper, A.K., 1995. Effect of high salt concentrations on water structure. Nature 378 (6555), 364–366.

Lee, S., Sigmund, W.M., 2002. AFM study of repulsive van der Waals forces between Teflon AF™ thin film and silica or alumina. Colloids Surf A Physicochem Eng Asp 204, 43–50.

Leroy, P., Jougnot, D., Revil, A., Lassin, A., Azaroual, M., 2012. A double-layer model of the gas bubble/water interface. J. Colloid Interface Sci. 388 (1), 243–256.

Liu, W., Moran, C.J., Vink, S., 2013. A review of the effect of water quality on flotation. Miner. Eng. 53, 91–100.

Manono, M.S., Corin, K.C., 2022. Considering Specific Ion Effects on froth stability in sulfidic Cu-Ni-PGM ore flotation. Minerals 12, 321.

Marrucci, G., Nicodemo, L., 1967. Coalescence of gas bubbles in aqueous solutions of inorganic electrolytes. Chem. Eng. Sci. 22 (9), 1257–1265.

Moignard, M.S., James, R.O., Healy, T.W., 1977. Adsorption of calcium at the zinc sulphide-water interface. Aust. J. Chem. 30, 733–740.

Morey, M.S., Grano, S.R., Ralston, J., Prestidge, C.A., Verity, B., 2001. The electrochemistry of PbII activated sphalerite in relation to flotation. Miner. Eng. 14 (9), 1009–1017.

Muster, T.H., Toikka, G., Hayes, R.A., Prestidge, C.A., Ralston, J., 1996. Interactions between zinc sulphide particles under flotation-related conditions. Colloids Surf. A Physicochem. Eng. Asp. 106 (2-3), 203–211.

Nguyen, A.V., Schulze, H.J., 2004. Colloidal Science of Flotation. Marcel Dekker, New York.
Nowosielska, A.M., Nikoloski, A.N., Parsons, D.F., 2022. A theoretical and experimental study of the effects of NaCl and the competitive chemisorption of ions at the surface sites in the context of galena flotation. Miner. Eng. 182, 107540.
October, L.L., Corin, K.C., Manono, M.S., Schreithofer, N., Wiese, J.G., 2020. A fundamental study considering specific ion effects on the attachment of sulfide minerals to air bubbles. Miner. Eng. 151, 106313.
October, L.L., Manono, M.S., Wiese, J.G., Schreithofer, N., Corin, K.C., 2021. Fundamental and flotation techniques assessing the effect of water quality in bubble-particle attachment of chalcopyrite and galena. Miner. Eng. 167, 106880.
Ozdemir, O., Du, H., Karakashev, S.I., Nguyen, A.V., Celik, M.S., Miller, J.D., 2011. Understanding the role of ion interactions in soluble salt flotation with alkylammonium and alkylsulfate collectors. Adv. Colloid Interface Sci. 163 (1), 1–22.
Parolis, L.A., Groenmeyer, G.V., Harris, P.J., 2008. The influence of metal cations on the behaviour of carboxymethyl celluloses as talk depressant. Colloids Surf. 317, 109–115.
Parsons, D.F., Ninham, B.W., 2012. Nonelectrostatic ionic forces between dissimilar surfaces: A mechanism for colloid separation. J. Phys. Chem. C 116 (14), 7782–7792.
Parsons, D.F., Salis, A., 2015. The impact of competitive adsorption of ions at surface sites on surface free energies and surface forces. J. Chem. Phys. 142.
Parsons, D.F. and Salis, A. (2019). A thermodynamic correction to the theory of competitive chemisorption of ions at surface sites with nonelectrostatic physisorption. *The Journal of Chemical Physics* ***151***.
Pugh, R.J., Weissenborn, P., Paulson, O., 1997. Flotation in inorganic electrolytes; the relationship between recover of hydrophobic particles, surface tension, bubble coalescence and gas solubility. Int. J. Miner. Process. 51 (1-4), 125–138.
Takagishi, H., Masuda, T., Shimoda, T., Maezono, R., Hongo, K., 2019. Method for calculation of the Hamaker constants of organic materials by the Lifshitz macroscopic approach with Density Functional Theory. J. Phys. Chem. 123, 8726–8733.
Trahar, W.J., Senior, G.D., Heyes, G.W., Creed, M.D., 1997. The activation of sphalerite by lead—a flotation perspective. Int. J. Miner. Process. 49 (3-4), 121–148.
Verwey, E.J.W., Overbeek, J.T.G., 1948. Theory of stability Lyophobic Colloids. Elsevier, Amsterdam.
Wang, B.O., Peng, Y., 2014. The effect of saline water on mineral flotation- a critical review. Miner. Eng. 66–68, 13–24.
Williams, R., Labib, M.E., 1985. Zinc sulfide surface chemistry: An electrokinetic study. J. Colloid Interface Sci. 106 (1), 251–254.
Wu, Z., Wang, X., Liu, H., Zhang, H., Miller, J.D., 2016. Some physicochemical aspects of water-soluble mineral flotation. Adv. Colloid Interface Sci. 235, 190–200.
Yang, C., Dabros, T., Li, D., Czarnecki, J., Masliyah, J.H., 2001. Measurement of the Zeta Potential of Gas Bubbles in Aqueous Solutions by Microelectrophoresis. J. Colloid Interface Sci. 243, 128–135.
Yoon, R.H., Sabey, J.B., 1989. Coal flotation in inorganic salt solution. In: Botsaris, G.G., Glazman, Y.M. (Eds.), Interfacial phenomena in Coal Technology. Marcel Dekker, New York.
Zhang, J., 2020. Applying high salinity water in flotation – A review. Aspects Min. Miner. Sci. 5 (1), 557–560.